Correlation between magnetism and lattice dynamics for cubic FeGe under pressure

OPEN ACCESS
IOP Publishing
Journal of Physics: Condensed Matter
J. Phys.: Condens. Matter **37** (2025) 465801 (9pp)
https://doi.org/10.1088/1361-648X/ae177c

Correlation between magnetism and lattice dynamics for cubic FeGe under pressure

R-A Tonacatl-Monez[1], R Heid[2] and O De la Peña-Seaman[1,*]

[1] Instituto de Física 'Ing. Luis Rivera Terrazas', Benemérita Universidad Autónoma de Puebla, Av. San Claudio & Blvd. 18 Sur, Ciudad Universitaria, C.P. 72570 Puebla, Puebla, Mexico
[2] Institut für QuantenMaterialien und Technologien, Karlsruher Institut für Technologie (KIT), D-76021 Karlsruhe, Germany

E-mail: omar.seaman@correo.buap.mx

Received 24 July 2025, revised 10 October 2025
Accepted for publication 24 October 2025
Published 11 November 2025

Abstract

This first-principles study investigates the structural, electronic, lattice dynamical properties, and electron–phonon coupling in ferromagnetic (FM) cubic B20 FeGe under applied pressure. The implemented spin-scaling exchange-correlation (ssxc) approach allowed to modify the magnetic moment and FM phase energetics using a single scaling parameter, thereby yielding an adjustment of the critical pressure (p_c) to its experimental value. The ssxc scheme resulted in a subtle energy shift of the electronic bands in the spin-up channel, and reduced the magnetic moment, bringing it closer to the experimentally reported value. Application of the ssxc approach to phonon dispersion and electron–phonon interaction resulted in a slight mitigation of the pronounced softening and large linewidths of the lowest-frequency acoustic branch close to the *R*-point, typically observed with standard density functional theory calculations. With increasing pressure, phonon anomaly and linewidths diminish significantly and practically disappear at p_c and beyond. This trend parallels the pressure dependence of the magnetic moment. A comparative analysis of the electronic joint density of states with the phonon linewidths revealed that the momentum dependence of linewidths around the *R*-point closely follow the momentum dependence of the electron–phonon matrix elements. This indicates that the correlation between magnetic moment and linewidths under applied pressure originates from the electron–phonon matrix elements, presenting a distinct scenario compared to other B20 family members, where nesting plays a more dominating role.

Keywords: first-principles calculations, lattice dynamics, magnetism, electron–phonon coupling, pressure

* Author to whom any correspondence should be addressed.

1. Introduction

Transition metals (Mn, Fe, Co) together with group 14 elements (Si, Ge) form compounds that can crystallize in two polymorphs with hexagonal B35 (space group P6/mmm, #191) and cubic B20 structure (space group $P2_13$, #198), that interestingly lacks inversion symmetry. These systems are of interest for technological development due to their magnetic properties, such as helical spin ordering and the presence of skyrmionic phases for the B20 structures, which show great potential for spintronics applications [1, 2]. Notable examples of B20 systems that have attracted significant interest include FeSi [3], MnSi [4], FeGe [5, 6], and the $Fe_{1-x}Co_xSi$ solid solution [7].

In particular, FeSi has been under intense investigation due to the temperature-dependent behavior of its electronic, transport, and magnetic properties [8, 9]. Furthermore, a strong temperature dependence of its phonon spectra has been observed, specifically an anomalous softening of low-frequency phonon modes along the [111] high-symmetry direction (close to the R-point), around 100 K, which corresponds to a crossover from a low-temperature non-magnetic (NM) ground state to a state with an induced paramagnetic moment [10, 11]. This phenomenon, along with drastic changes in the related phonon linewidths that follow the observed magnetization trends with temperature, clearly indicates a correlation between magnetism and lattice dynamic properties in FeSi [12–14]. This interplay between magnetic order and lattice dynamics is not unique to FeSi. For instance, in MnSi, substitutional doping with Fe ($Mn_{1-x}Fe_xSi$) leads to the suppression of its helical magnetic order, reaching a magnetic critical point at a critical concentration of $x_c = 0.17$ [15]. Interestingly, this system also exhibits a significant softening and broadening of a low-frequency phonon mode along the [111] direction with an increasing Fe-content, a phenomenon linked to changes in the Fermi surface geometry [16].

A similar behavior of the low-frequency phonon modes along the same direction of FeSi and $Mn_{1-x}Fe_xSi$ (both at its magnetic phase) is also observed in ferromagnetic (FM) first-principles calculations for cubic FeGe [17]. The B20 cubic polymorph is stable below 853 K, while above this temperature the hexagonal structure is preferred [18]. In the B20 structure, FeGe has a long-range helical spin structure, along the [111] direction, below a critical temperature of $T_c \sim 280$ K [5]. Near T_c its characteristic helical magnetic order transits to a conical one as the applied magnetic field raises, reaching a skyrmion phase (swirling spin texture) for a specific region of magnetic field and temperature [19]. Unlike FeSi, FeGe experimentally exhibits a reduction of the magnetic moment (from $3.928 \pm 0.007 \mu_B$ per unit cell) as the temperature increases up to T_c, where it undergoes a magnetic to non−magnetic phase transition [20, 21]. However, neither experimental nor theoretical work exists addressing the question, if the phonon softening predicted for the FM phase also persists into the NM high-temperature phase. In addition to modifying the FeGe magnetic phase by temperature, as in FeSi, or by doping, like $Mn_{1-x}Fe_xSi$, experimental studies show a reduction of the magnetic moment as a function of applied pressure. In particular, the observed long-range helical magnetism (typical of B20 materials) disappears at approximately 19 GPa, reaching an inhomogeneous chiral spin state which finally changes to the paramagnetic state at a critical pressure (p_c) value of 28.5 GPa [22]. There have been attempts to reproduce the observed p_c value through first-principles studies, yielding a wide range of values, from 10 GPa to 40 GPa with local-density approximation and generalized gradient approximation (GGA) (PW91) functionals, respectively [23]. Clearly, such reported values differ from the experimentally determined one, although the FeGe structural ground-state properties are reasonably well described.

Thus, the aim of this work is twofold for FeGe: first, analyze a different methodological approach to properly describe the critical pressure at which the magnetic transition takes place and sense its influence on the electronic and lattice dynamical properties, and second, to analyze the evolution of the lattice dynamics (phonon frequencies and linewidths) as a function of pressure. This analysis aims to determine if there is any correlation between magnetism and lattice dynamics, similar to what is observed in FeSi or $Mn_{1-x}Fe_xSi$, by using applied pressure, instead of temperature or doping content, as a method to modulate magnetism in the system.

2. Methodology

First-principles calculations were performed using density functional theory (DFT) [24, 25] implemented in the mixed-based pseudopotential method (MBPP) [26] and using the GGA by Perdew–Burke–Ernzerhof (PBE) [27] for the exchange and correlation functional, neglecting spin–orbit coupling. The NM calculations were considered to model the paramagnetic state. We are aware that the NM state does not take into account the localized magnetic moments present in the paramagnetic one. However, it represents an approximate description of the non-polarized electronic system. The magnetic phase was approximated by a collinear spin-polarized , i.e. FM phase, since the FeGe helical spin structure possesses a long pitch-period in comparison with the unit cell (approximately 150 times larger) [28]. Norm-conserving pseudopotentials for Fe and Ge were constructed using the Vanderbilt scheme [29], including semicore states Fe $3s$ and $3p$ in the valence region. Furthermore, s, p, and d local functions at Fe sites were added to the plane-wave expansion up to a kinetic energy of 24 Ry. For the integration of the Brillouin zone, the Monkhorst–Pack special k-point set technique was used, with a Gaussian smearing of 0.1 eV and a grid of $16 \times 16 \times 16$ for the crystal structural optimization, and a $48 \times 48 \times 48$ mesh for the electronic properties.

Phonon properties, that is, phonon dispersion and phonon density of states, were calculated via density functional perturbation theory (DFPT) [30, 31], implemented in the MBPP code [32]. Complete phonon dispersions were obtained via

standard Fourier interpolation of dynamical matrices calculated on a $4 \times 4 \times 4$ q-point mesh, on basis of a $16 \times 16 \times 16$ k-point grid. The differences in interpolation (phonon dispersion) were minimal (less than 0.4 meV) when comparing with denser meshes. For the calculation of electron–phonon (e–ph) coupling matrix elements, a denser k-point mesh of $48 \times 48 \times 48$ for the Brillouin sampling was required to achieve convergence. The reported numerical parameters were chosen such that frequencies were converged better than 0.05 meV, constituting a compromise between precision and computational cost.

The standard DFT spin-polarized (ssp) calculation tends to overestimate the ordered magnetic moment in the FM state especially for itinerant magnets, where spin fluctuations effectively weaken the magnetic interaction. An elegant method to amend this is the spin scaling exchange-correlation (ssxc) correction [33–35]. This scheme introduces a linear scaling of the magnetization density and potential in the evaluation of the exchange-correlation potential by a single scaling parameter (s), while the charge potential remains unchanged. It can be interpreted as a scaling of the effective Stoner parameter, which characterizes the strength of the magnetic interaction [33]. This scheme is variational and adapts the spin polarization for all standard types of exchange-correlation functionals in a self-consistent way. A value $s = 1$ corresponds to the standard ssp calculation. This approach has previously been applied to the $Mn_{1-x}Fe_xSi$ solid solution [16], where it successfully described a significant reduction of the ordered magnetic moment, while the LDA + U method required unrealistic high values of $U > 6 - 7$ eV to achieve the same reduction [36, 37].

3. Results and discussion

3.1. Structural properties

The B20 crystal structure is cubic with four formula units (f.u.) within the unit cell, where its Wyckoff atomic positions ($4a$) are given by the coordinates (u, u, u), $(0.5 + u, 0.5 - u, -u)$, $(-u, 0.5 + u, 0.5 - u)$ and $(0.5 - u, -u, 0.5 + u)$ [28]. The FeGe lattice structure was fully optimized by determining the total energy for a set of volumes. For a given volume, the internal coordinates u_{Fe} and u_{Ge} were optimized by force minimization, with a force threshold of 0.005 Ry/a.u. Results for $E(V)$ were then fitted to the Birch–Murnaghan equation of state (EOS) [38], from which the optimized structure as well as the relation $p(V)$ were extracted. Optimized structural parameters for the NM and FM phases are shown in table 1, along with the corresponding magnetic moment (m) per unit cell. Values for the FM state do agree nicely with available experimental data [28, 39, 40], but the magnetic moment is overestimated by about 10%.

The critical pressure (p_c) where the magnetic transition from FM to NM takes place, is determined by comparing the enthalpy $H(p) = E(V) + pV$ for both phases as a function of pressure. In figure 1(a) the enthalpy difference (ΔH) between

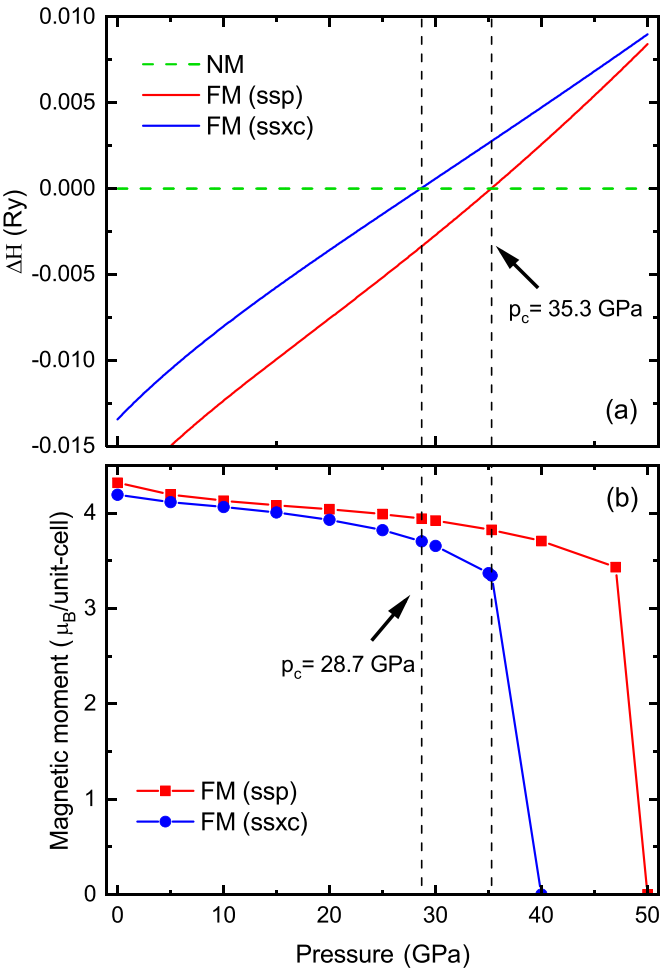

Figure 1. Evolution of (a) the enthalpy difference (between NM and FM phases) as a function of pressure, where a negative value indicates a more stable magnetic phase, and (b) magnetic moment for the FM ssp and ssxc schemes. The vertical lines indicate the critical pressure (p_c): 28.7 GPa for ssxc with $s = 0.979$, and 35.3 GPa for ssp.

the FM and NM phases is presented. For low pressures, ΔH is negative indicating the stability of the FM state. The sign change of ΔH signals the phase transition from FM to NM as function of pressure and determines p_c. From this analysis, $p_c = 35.3$ GPa was determined for the ssp scheme, which differs considerably from the experimental value of 28.5 GPa [22].

In order to improve the critical-pressure value, the spin scaling exchange-correlation (ssxc) correction was employed [33–35]. Figure 2 shows the dependence of p_c and the magnetic moment m at $p = 0$ GPa on the scaling parameter s. The critical pressure is very sensitive to s, reaching the experimental value with a moderate reduction to $s = 0.979$. Simultaneously, the magnetic moment for $p = 0$ GPa is also improved, showing a difference of roughly 6% with respect to the experimental value (see table 1).

The evolution of the magnetic moment as a function of pressure obtained by both schemes, ssp and ssxc (with

Table 1. The optimized structural parameters, in particular the volume (V_0), bulk modulus (B_0), and lattice internal parameters (u) for Fe and Ge, for the NM and FM phases at ambient pressure. Shown is also the magnetic moment m (per unit cell) without applied pressure and the critical pressure p_c for the standard spin-polarized case (ssp) and for the spin-scaling exchange-correlation correction (ssxc) with $s = 0.979$. The last column indicates the calculated magnetic moment at p_c.

	V_0 (Bohr^3)	B_0 (GPa)	u (Fe)	u (Ge)	m (μ_B)	p_c (GPa)	$m@p_c$ (μ_B)
NM	677.48	170.23	0.13 335	0.83 842	–	–	–
FM-ssp	687.99	149.43	0.13 495	0.84 178	4.31	35.3	3.82
FM-ssxc	686.85	156.74	0.13 493	0.84 173	4.19	28.7	3.70
Exp.	700.63 [39]	147.00 [39]	0.13 524 [28]	0.8414 [28]	3.928 [20]	28.5 [22]	–

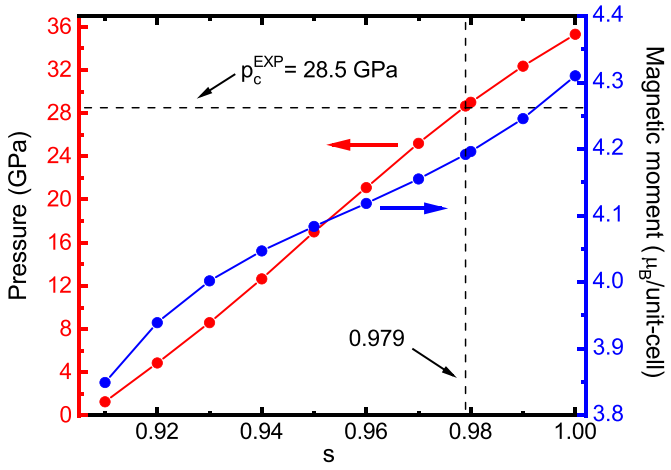

Figure 2. Determined critical pressure (p_c) and magnetic moment as a function of the ssxc parameter s. The dotted horizontal line indicates the experimental p_c value [22].

$s = 0.979$), is compared in figure 1(b). Trends are qualitatively similar, but with a reduced pressure range for the FM phase and with slightly smaller magnetic moments in the case of the ssxc sheme. It is important to mention that there are still magnetic solutions for FeGe at pressure values above p_c for both schemes. However, as can be seen from the enthalpy difference in figure 1(a), these FM solutions are energetically less favorable than the NM state, representing metastable states. Thus the pressure induced transition from FM to NM is predicted to be of first order. Interestingly, the structural properties obtained by the ssxc scheme with $s = 0.979$ differ only marginally from those obtained by the ssp scheme, as can be seen in table 1, indicating that both schemes equally well describe the experimental data.

3.2. Electronic properties

The band structure and density of states (DOS) for FM FeGe, without applied pressure ($p = 0$ GPa), are shown in figure 3 for the spp and ssxc with $s = 0.979$, respectively, to elucidate the effects of spin-scaling on its electronic properties. In general, the spin-down channel possesses a higher value of the density of states at the Fermi level, $N(E_F)$, as compared to the spin-up channel. In particular, the spin-down channel does not show any visible effects when using the ssxc approach, while that is not the case for the spin-up channel, where ssxc leads to a slight shift in the bands and DOS towards higher energies than ssp. Since the ssxc scheme scales down the exchange potential and reduces the magnetic moment, it tends to reduce the original exchange splitting between spin channels. Due to the larger $N(E_F)$ for the spin-down channel as compared to the spin-up channel, the spin-down channel essentially pins the Fermi energy, while the spin-up bands shift relative to E_F. Atom-resolved DOS for the FM state of FeGe at ambient pressure are presented in Figure 4 for the ssxc scheme, using $s = 0.979$. For both spin channels, the larger contribution is due to Fe-d orbitals, with much lower participation of Ge states, mainly coming from d and p orbitals.

To illustrate the effect of pressure on the electronic structure, figure 5 presents the DOS for two different pressures, calculated with ssxc ($s = 0.979$). For the spin-up channel, there is a shift toward higher energy values, while the opposite is observed for the spin-down channel, that is, a shift to lower energy values with respect to the Fermi level, especially for states below 1 eV. This behavior is understood by the tendency to reduce the magnetic moment of FM FeGe and to approach the NM solution as the pressure increases.

The evolution of the density of states at the Fermi level ($N(E_F)$) as a function of pressure, for each spin channel, is presented in figure 6 for both schemes, ssp and ssxc

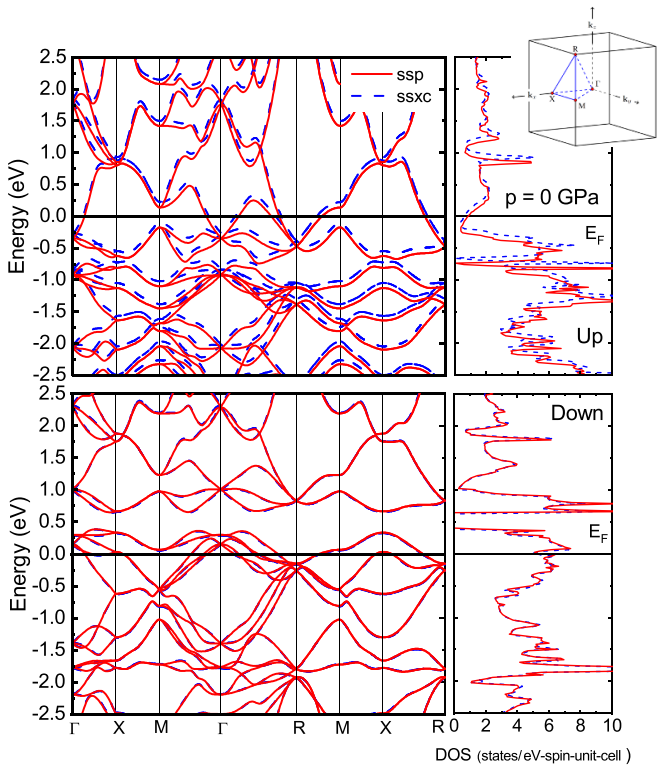

Figure 3. Electronic band structure and density of states of FM FeGe ($p = 0$ GPa), for both spin-channels, comparing ssp and ssxc (with $s = 0.979$) schemes. The related first Brillouin of the simple cubic structure zone is presented as an inset.

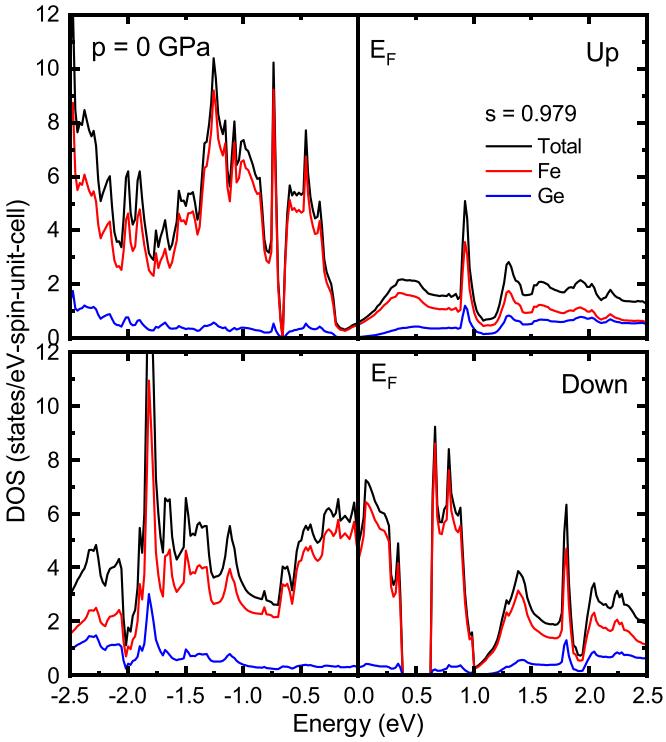

Figure 4. Spin-polarized density of states (DOS) for FM FeGe, obtained with the ssxc scheme (using $s = 0.979$) without applied pressure, showing the contribution by atom (in the unit cell).

($s = 0.979$). In general, both schemes show not only the same trend as a function of pressure, but also agree quantitatively for a wide range of applied pressure. Differences start to appear as one approaches p_c. The smaller p_c value for ssxc results in a shrinking of the pressure range. However, independent of the spin channel, the $N(E_F)$ differences between the schemes are not very large, even for pressures close to p_c, indicating that spin-scaling induces only subtle changes in the electronic properties.

3.3. Lattice dynamical properties and e–ph coupling

To study the sensitivity of phonons and e–ph coupling with respect to the magnetic order, in particular with respect to the magnetic moment, phonon dispersion and linewidths were calculated for four cases with different magnetic moments, obtained by changing the s parameter: 4.31 μ_B ($s = 1$), 4.19 μ_B ($s = 0.979$), 4.0 μ_B ($s = 0.930$), and the NM case (0 μ_B) for comparison. The first one corresponds to the standard spin-polarized calculation (ssp), and the second one to the s value that fits the critical pressure to the experimental data. The third one uses an even smaller s value to further suppress the magnetic moment, while the last one corresponds to the non-spin polarized case. All calculations were done for their corresponding optimized structures at $p = 0$ GPa. The ssp scheme shows a phonon anomaly close to the R-point in the acoustic branches, as previously noted [17], while the corresponding linewidths are, by far, the largest ones in the whole phonon spectra. With decreasing magnetic moment, the frequencies of all phonons increase, but the most prominent modification is a drastic hardening of the low-frequency acoustic phonon branches in the neighborhood of the R-point, accompanied by a reduction of their linewidths. In particular, the lowest-frequency mode at the R-point exhibits a clear correlation between phonon hardening and linewidth reduction (see figures 7(a) and (b)). Branches attached to this mode also show the highest sensitivity to changes in the ordered magnetic moment. For example, when going from the $s = 1$ to the $s = 0.979$ case, the phonon anomaly as well as the corresponding linewidths are visibly downsized, despite an only 3% difference between their corresponding magnetic moments.

Phonon dispersions and linewidths for the FM phase with a scaling parameter $s = 0.979$ are presented for several pressure values in figure 8. Increasing pressure generally hardens the phonon frequencies, which is particularly evident for the acoustic branches in the $\Gamma - R$ path where the phonon anomaly is present at $p = 0$ GPa. This phonon renormalization is notably stronger in the pressure range where the FM phase is the more stable one, that is, for pressure values lower than $p_c = 28.7$ GPa.

For the analysis of the phonon linewidth, $\gamma_{\mathbf{q}\eta}$, we recall that it is expressed as

$$\gamma_{\mathbf{q}\eta} = 2\pi\omega_{\mathbf{q}\eta} \sum_{\mathbf{k}\nu\nu'} \left| g^{\mathbf{q}\eta}_{\mathbf{k}+\mathbf{q}\nu',\mathbf{k}\nu} \right|^2 \delta\left(\epsilon_{\mathbf{k}\nu} - E_F\right) \delta\left(\epsilon_{\mathbf{k}+\mathbf{q}\nu'} - E_F\right), \quad (1)$$

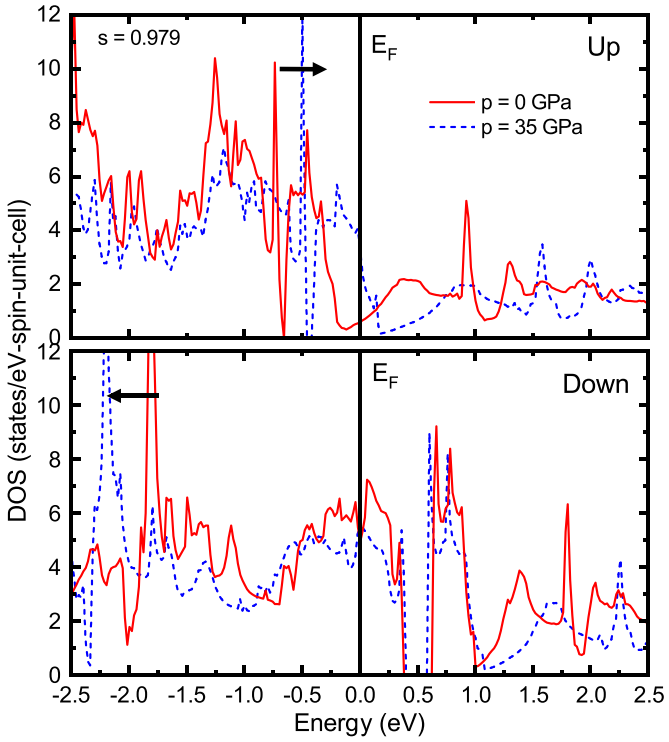

Figure 5. Spin-polarized DOS of two different applied pressure values, 0 GPa and 35 GPa, calculated under the ssxc scheme with $s = 0.979$.

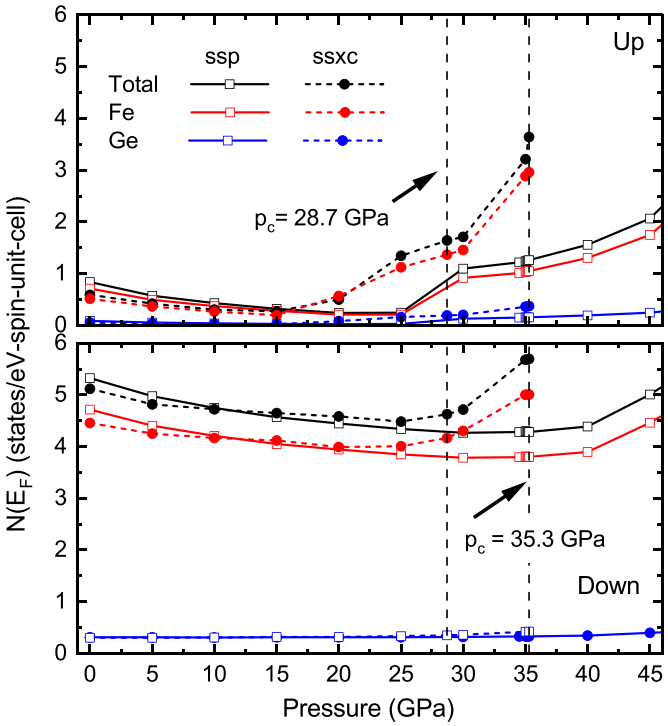

Figure 6. Evolution of the density of states at the Fermi level, $N(E_F)$, as a function of applied pressure for FM FeGe, separated by atomic contribution and calculated with both schemes, ssp and ssxc ($s = 0.979$). The dotted vertical lines represent the critical pressure value obtained for each scheme: 28.7 GPa for ssxc, and 35.3 GPa for ssp.

where $\omega_{\mathbf{q}\eta}$ is the frequency of the phonon mode at the $\mathbf{q}$ vector and branch η, and $\epsilon_{\mathbf{k}\nu}$ is the one-electron band energy with momentum $\mathbf{k}$ and band index ν. $\gamma_{\mathbf{q}\eta}$ is closely related to the electronic joint density of states (eJDOS), given by $\sum_{\mathbf{k}\nu\nu'} \delta(\epsilon_{\mathbf{k}\nu} - E_F)\,\delta(\epsilon_{\mathbf{k}+\mathbf{q}\nu'} - E_F)$, but with the difference that the sum is weighted by squared e–ph coupling matrix elements $g^{\mathbf{q}\eta}_{\mathbf{k}+\mathbf{q}\nu',\mathbf{k}\nu}$. We explicitly calculated eJDOS (which is also referred as the Fermi surface nesting function) to discriminate between the influence of e–ph coupling matrix elements and Fermi surface geometry on the linewidths. The same k-mesh and broadening parameters were used as in the linewidth calculation. Since the FeGe ground state is spin polarized, the eJDOS is also spin dependent. However, due to its low $N(E_F)$, the contribution from the spin-up channel is almost negligible in comparison with the spin-down channel (a couple of orders of magnitude smaller, not shown here). Thus, we present only the results for the spin-down channel in figure 9 together with the linewidth of the corresponding lowest-frequency acoustic branch in the Γ-R path. Additionally, the ratio between $\gamma_{\mathbf{q}}$ and eJDOS is presented, which defines an average of the momentum-dependent e–ph coupling matrix elements.

From the $p = 0$ GPa case (see figure 9), it is clear that the linewidth is significantly larger as $\mathbf{q}$ approaches the R-point. As pressure increases, with a simultaneous decrease of the magnetic moment, the linewidth starts to decrease and practically disappears for $p \geqslant p_c$. Although eJDOS shows a slight shoulder around the R-point throughout the analyzed pressure

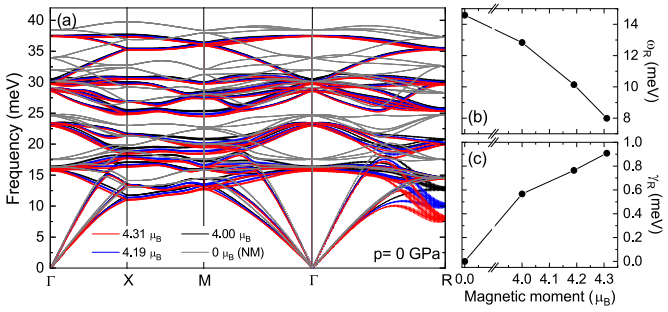

Figure 7. (a) Comparison of phonon dispersion and linewidths (phonon branches width), without applied pressure, for several magnetic cases: 4.31 μ_B (ssp), 4.19 μ_B ($s = 0.979$), 4.0 μ_B ($s = 0.930$), and 0 μ_B (NM). Evolution as a function of magnetic moment of (b) frequency and (c) linewidth for the lowest-frequency mode at the R-point.

range, it is unclear whether the linewidth behavior is related to nesting features. However, the $\gamma_{\mathbf{q}}$/eJDOS ratio, which, as stated before, is a measure of the $\mathbf{q}$-dependent e–ph coupling matrix elements, closely follows the same behavior as the linewidth: a steady increase as $\mathbf{q}$ approaches the R-point, and a drastic reduction as the applied pressure increases and the magnetic moment decreases. Thus, large linewidth values around the R-point for the lowest-frequency acoustic branch

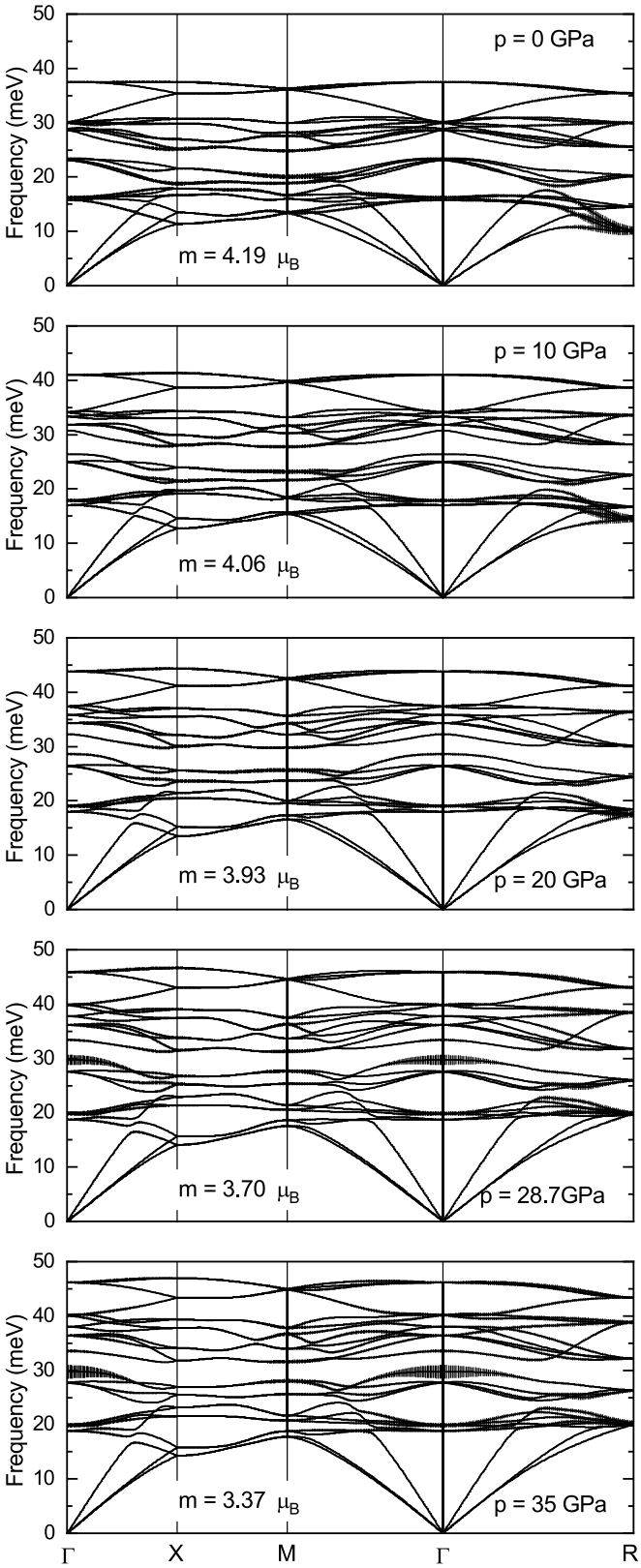

Figure 8. Phonon dispersion and linewidths calculated for the FM ssxc scheme ($s = 0.979$) at several applied pressure values.

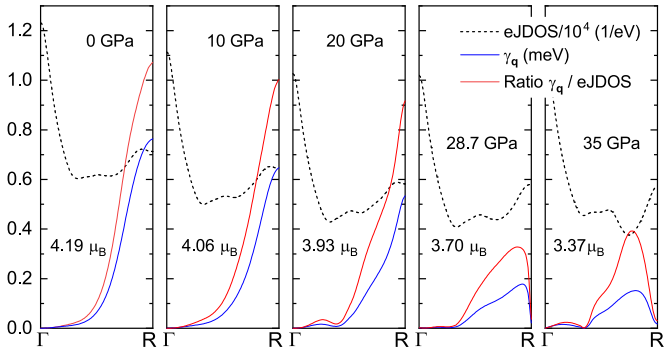

Figure 9. Comparison of eJDOS (scaled), phonon linewidth of the lowest-frequency acoustic branch $\gamma_{\mathbf{q}}$, and the ratio of $\gamma_{\mathbf{q}}$ and eJDOS, which describes an average of the $\mathbf{q}$-dependent e–ph coupling matrix elements, for several pressure values, calculated under the ssxc scheme with $s = 0.979$.

are linked to presence of magnetism, and originates in a significant increase of e–ph coupling matrix elements in this region.

4. Conclusion

As a summary, we have performed a first-principles study on the structural, electronic, lattice dynamical properties, and e–ph coupling of FM cubic FeGe as a function of applied pressure. Implementing the spin-scaling exchange-correlation (ssxc) approach, allowed us to adjust the critical pressure, p_c, to the experimental value. A small reduction of the scaling parameter from $s = 1$ to $s = 0.979$ was sufficient to reduce the magnetic moment and the energetics of the FM phase to yield a proper p_c value. The spin-scaling correction essentially affects the energetic position of the spin-up bands only. Subsequently, using the ssxc scheme, at a fixed scaling parameter $s = 0.979$, we analyzed the evolution of the phonon dispersion, $\omega_{\mathbf{q}}$, and linewidths, $\gamma_{\mathbf{q}}$, as a function of applied pressure. Firstly, we observed that the pronounced softening and large linewidths at the R-point, obtained by standard DFT calculations, are lessened by the ssxc scheme, which reduces at the same time the magnetic moment. Secondly, the phonon anomaly and associated large linewidth values diminished with increasing pressure, practically disappearing beyond p_c. To understand the origin of this behavior, we compared the eJDOS, $\gamma_{\mathbf{q}}$, and the average of the momentum-dependent e–ph coupling matrix elements (obtained through the $\gamma_{\mathbf{q}}$/eJDOS ratio) for the lowest-frequency acoustic branch in the Γ-R path. With increasing pressure, we found very similar trends between $\gamma_{\mathbf{q}}$ and this ratio as $\mathbf{q}$ approaches the R-point, with a simultaneous reduction of the magnetic moment. These findings strongly suggest that the observed correlation between the decrease in the magnetic moment and the reduction in linewidths with applied pressure has its origin in significant changes of the e–ph coupling matrix elements. This represents a mechanism distinct to other members of the B20 family, such as the $Mn_{1-x}Fe_xSi$ solid solution, where doping induced changes in linewidths are dominated by changes in the Fermi surface geometry, i.e. nesting.

Data availability statement

All data that support the findings of this study are included within the article (and any supplementary files).

Acknowledgments

This research was partially supported by Vicerrectoría de Investigación y Estudios de Posgrado (VIEP), Benemérita Universidad Autónoma de Puebla (BUAP) under Grant No. 100517450-VIEP2025, the Deutscher Akademischer Austausch Dienst (DAAD), and the Karlsruher Institut für Technologie (KIT), Germany. One of the authors (R A T M) gratefully acknowledges financial support from the Secretaría de Ciencia, Humanidades, Tecnología e Innovación (Secihti, México).

Author contributions

R-A Tonacatl-Monez
Formal analysis (equal), Investigation (equal), Methodology (equal), Software (equal), Visualization (equal), Writing – original draft (equal)

R Heid
Methodology (equal), Software (equal), Validation (equal), Writing – review & editing (equal)

O De la Peña-Seaman 0000-0001-6590-3807
Conceptualization (lead), Data curation (lead), Funding acquisition (lead), Project administration (lead), Resources (equal), Supervision (lead), Writing – original draft (equal), Writing – review & editing (lead)

References

[1] Kiselev N, Bogdanov A, Schäfer R and Rößler U 2011 *J. Phys. D: Appl. Phys.* **44** 392001
[2] Kanazawa N 2015 *Charge and Heat Transport Phenomena in Electronic and Spin Structures in B20-Type Compounds* (Springer)
[3] Eo Y S, Avers K, Horn J A, Yoon H, Saha S R, Suarez A, Fuhrer M S and Paglione J 2023 *Appl. Phys. Lett.* **122** 233102
[4] Ishikawa Y, Tajima K, Bloch D and Roth M 1976 *Solid State Commun.* **19** 525–8
[5] Grigoriev S V *et al* 2014 *Phys. Rev. B* **90** 174414
[6] Wang K, Wei W and Du H 2025 *Adv. Funct. Mater.* **35** 2416203
[7] Kanazawa N, Shibata K and Tokura Y 2016 *New J. Phys.* **18** 045006
[8] Schlesinger Z, Fisk Z, Zhang H T, Maple M, DiTusa J and Aeppli G 1993 *Phys. Rev. Lett.* **71** 1748
[9] Buschinger B, Geibel C, Steglich F, Mandrus D, Young D, Sarrao J and Fisk Z 1997 *Phys. B* **230** 784
[10] Jaccarino V, Wertheim G, Wernick J, Walker L and Arajs S 1993 *Phys. Rev.* **160** 476
[11] Mandrus D, Sarrao J, Migliori A, Thompson J and Fisk Z 1995 *Phys. Rev. B* **51** 4763
[12] Menzel D, Popovich P, Kovaleva N N, Schoenes J, Doll K and Boris A V 2009 *Phys. Rev. B* **79** 165111

[13] Delaire O, Marty K, Stone M, Kent P, Lucas M, Abernathy D, Mandrus D and Sales B 2011 *Proc. Natl Acad. Sci.* **108** 4725–30
[14] Krannich S *et al* 2015 *Nat. Commun.* **6** 8961
[15] Bannenberg L, Dalgliesh R, Wolf T, Weber F and Pappas C 2018 *Phys. Rev. B* **98** 184431
[16] Khan N *et al* 2024 *Phys. Rev. B* **109** 184306
[17] Khan M A *et al* 2016 *Phys. Rev. B* **94** 144424
[18] Stolt M, Sigelko X, Mathur N and Jin S 2018 *Chem. Mater.* **30** 1146
[19] Yu X, Kanazawa N, Onose Y, Kimoto K, Zhang W, Ishiwata S, Matsui Y and Tokura Y 2011 *Nat. Mater.* **10** 106
[20] Spencer C S *et al* 2018 *Phys. Rev. B* **97** 214406
[21] Wilhelm H, Baenitz M, Schmidt M, Rößler K, Leonov A A and Bogdanov A N 2011 *Phys. Rev. Lett.* **107** 127203
[22] Barla A, Wilhelm H, Forthaus M, Strohm C, Rüffer R, Schmidt M, Koepernik K, Rößler U and Abd-Elmeguid M 2015 *Phys. Rev. Lett.* **114** 016803
[23] Neef M, Doll K and Zwicknagl G 2009 *Phys. Rev. B* **80** 035122
[24] Hohenberg P and Kohn W 1964 *Phys. Rev.* **136** B864
[25] Kohn W and Sham L J 1965 *Phys. Rev.* **140** A1133
[26] Meyer B, Elsässer C, Lechermann F and Fähnle M FORTRAN90 Program for Mixed-Basis Pseudopotential Calculations for Crystals, Max-Planck-Institut für Metallforschung, Sttutgart (unpublished)
[27] Perdew J, Burke K and Ernzerhof M 1996 *Phys. Rev. Lett.* **77** 3865
[28] Lebech B, Bernhard J and Freltoft T 1989 *J. Phys.: Condens. Matter* **1** 6105
[29] Vanderbilt D 1985 *Phys. Rev. B* **32** 8412
[30] Louie S, Ho K and Cohen M 1979 *Phys. Rev. B* **19** 1774
[31] Baroni S, Gironcoli S D and Corso A D 2001 *Phys. Rev. Lett.* **73** 515
[32] Heid R and Bohnen K P 1999 *Phys. Rev. B* **60** R3709
[33] Ortenzi L, Mazin I I, Blaha P and Boeri L 2012 *Phys. Rev. B* **86** 064437
[34] Onuorah I, Bonfá P and Renzi R D 2018 *Phys. Rev. B* **97** 174414
[35] Sharma S, Gross E, Sanna A and Dewhurst J 2018 *Chem. Theory Comput.* **14** 1247
[36] Collyer R and Browne D A 2008 *Physica B* **403** 1420
[37] Dutta P and Pandey S 2018 *Comput. Condens. Matter* **16** e00325
[38] Birch F 1947 *Phys. Rev.* **71** 809
[39] Pshenay-Severin D and Burkov A 2019 *Materials* **17** 12
[40] Pedrazzini P *et al* 2007 *Phys. Rev. Lett.* **98** 047204